Dynamin regulates PLK-1 localization and spindle pole assembly during mitosis

Carter Dierlam[1], Livinus Anyanwu[2§], Stephanie Held[3§], Robert H. Newman[3], and Jyoti Iyer[3]*

[1]Department of Cell Biology and Molecular Genetics, University of Maryland College Park, College Park, MD 20742,[2]Department of Chemistry and Biochemistry, University of Tulsa, Tulsa, OK 74104 and [3]Department of Biology, North Carolina Agricultural and Technical State University, Greensboro, NC 27411.

[§]Equal Contribution

Number of characters = 19,800

Running title: *DYN-1 regulates PLK-1 localization*

To whom correspondence should be addressed:

Jyoti Iyer

Email: jgiyer@ncat.edu; Tel. (336) 285-4573

Keywords: dynamin, Plk1, mitosis, midbody, cytokinesis

ABSTRACT

Accurate cytokinesis is essential for maintaining genomic integrity. Although the GTPase dynamin has been well studied for its role in vesicular trafficking, its function during mitosis remains poorly understood. In this study, we uncover a novel role for the *C. elegans* dynamin homolog, DYN-1, in regulating mitotic spindle pole assembly and the spatiotemporal localization of the key mitotic kinase Polo-like kinase 1 (PLK-1). Our studies demonstrate that the depletion of DYN-1 leads to enlarged metaphase spindle poles and elevated levels of centrosome-associated PLK-1. Strikingly, PLK-1 fails to re-localize from centrosomes to the midbody during late mitosis in a subset of DYN-1–depleted embryos, correlating with abnormal PLK-1 localization at the midbody and defective midbody formation. Importantly, this phenotype is likely not due to increased total PLK-1 protein levels, as DNM2 (human homolog of DYN-1) depletion in HeLa cells did not alter total Plk1 abundance. Together, our findings identify DYN-1 as a new regulator of PLK-1 localization during mitosis and suggest that failure to remove PLK-1 from centrosomes may underlie cytokinesis defects that are observed upon DYN-1 depletion.

SIGNIFICANCE STATEMENT

Dynamin is primarily known for its function in endocytosis, but its involvement in mitosis is not well defined. This study shows that dynamin helps organize the mitotic spindle and ensures proper localization of the master mitotic kinase PLK-1 in *C. elegans* embryos. These findings reveal a previously unrecognized role for dynamin in mitosis and suggest new links between membrane dynamics and the cell division machinery.

41 **INTRODUCTION**

42 Proper cytokinesis is a prerequisite for the accurate partitioning of the chromosomes to
43 yield two genetically identical daughter cells. Cytokinesis defects can lead to aneuploidy, which
44 is a characteristic feature of cancer cells. Therefore, it is essential to understand the molecular
45 mechanisms governing cytokinesis. The GTPase dynamin is a large ~100 kDa protein that is best
46 known for its role in the scission of endocytic vesicles (Hinshaw JE 2000; Menon *et al.,* 2013;
47 Khurana *et al.,* 2023). The dynamin protein is strongly conserved between humans and the
48 multicellular eukaryotic nematode *Caenorhabditis elegans* (*C. elegans*). *C. elegans* have a single
49 classical dynamin isoform called DYN-1. There is over 60% identity at the amino acid level
50 between human DNM2 and *C. elegans* DYN-1 (Clustal Omega). Interestingly, some of the
51 earliest studies identified dynamin as a microtubule-binding protein (Shpetner and Vallee*,* 1989).
52 However, dynamin's function in microtubule-associated processes is less well understood.
53 Studies in various organisms including *C. elegans* and human cells have revealed that dynamin is
54 required for proper cytokinesis (Thompson *et al.,* 2002; Wienke *et al.,* 1999; Pelissier *et al.,*
55 2003). However, mechanistic gaps still exist in our understanding of how DNM2 regulates
56 cytokinesis.

57 Polo-like kinase 1 (Plk1) is a mitotic master regulator that is essential for several mitotic
58 processes including mitotic entry, centrosome dynamics, polarity establishment, chromosome
59 congression, chromosome alignment and cytokinesis (Petronczki *et al.,* 2008; Archambault and
60 Glover, 2009; Zitouni *et al.,* 2014, Nishi *et al.*, 2008). Importantly, Plk1 exhibits a dynamic
61 localization pattern at different stages of mitosis. During early mitosis, Plk1 localizes to the
62 centrosomes and the kinetochores. At anaphase, it re-localizes to the spindle midzone and at
63 telophase, it localizes to the midbody (Golsteyn *et al.,* 1995; Lee *et al.,* 1995; Arnaud *et al.,*

1998; Petronczki *et al.,* 2008; Kishi *et al.,* 2009; Schmucker and Sumara, 2014). The timely localization of Plk1 to various cellular components is essential for its different important roles during mitosis. Importantly, like DNM2, Plk1 is also required for proper cytokinesis (Petronczki *et al.,* 2008; Archambault and Glover, 2009; Zitouni *et al.,* 2014). Plk1 activity is required for recruitment of the RhoA guanine nucleotide exchange factor (GEF), Ect2, to the spindle midzone and equatorial cortex through phosphorylation of the centralspindlin component CYK4. Ect2, in turn, mediates RhoA activation to facilitate contractile ring assembly and cleavage furrow ingression, thereby ensuring proper cytokinesis (Brennan *et al.,* 2007; Burkard *et al.,* 2007; Petronczki *et al.,* 2007; Santamaria *et al.,* 2007; Petronczki *et al.,* 2008; Burkard *et al.,* 2009; Wolfe *et al.,* 2009). Importantly, removal of Plk1 from the centrosomes is required for proper mitotic progression (Kishi *et al.,* 2009). Although the kinase activity of Plk1 is thought to be required for Plk1 removal from the centrosomes (Kishi *et al.,* 2009), the mechanism by which Plk1 is removed from the centrosomes remains unclear.

RESULTS AND DISCUSSION

dyn-1 RNAi embryos exhibit cytokinesis defects

To study the role of DYN-1 in cytokinesis, we depleted endogenous DYN-1 from *C. elegans* embryos expressing mCherry-SPD-2 (marks centrosomes) and GFP-histone (marks DNA) using *RNAi*. Importantly, our *RNAi* procedure successfully reproduced the cytokinesis failure phenotype that was previously reported by Thompson *et al*. upon *dyn-1 RNAi* in *C. elegans* (Thompson *et al.,* 2002). While all of the control (S-adenosyl-methionine decarboxylase (*smd-1*)) *RNAi* treated embryos proceeded normally through cell division (n=28 embryos), 45% of the *dyn-1 RNAi* embryos failed cytokinesis (n=31 embryos) (Fisher's exact test, $p<0.0001$) **(Figure S1)**. Since our *RNAi* depletion was able to replicate the cytokinesis failure phenotype that was

previously reported upon *dyn-1 RNAi* in *C. elegans* by another group (Thompson *et al.,* 2002), we concluded that our depletion was successful. Therefore, we proceeded to investigate the downstream effects of DYN-1 depletion.

dyn-1 depletion results in abnormal metaphase spindle pole assembly

Interestingly, DYN-1 was shown to localize to the mitotic spindle at metaphase, suggesting a potential role in metaphase spindle assembly (Thompson *et al.,* 2002). To determine the effect of DYN-1 depletion on metaphase spindle assembly, we depleted DYN-1 using *RNAi* and examined the effect of DYN-1 depletion on metaphase spindle assembly using mCherry-tubulin as a proxy **(Figure 1)**. Upon measuring spindle pole area (as assessed by mCherry-tubulin fluorescence intensity), we determined that DYN-1-depleted embryos (n=58 spindle poles) exhibited a larger spindle pole area than control (*smd-1*) *RNAi* depleted embryos (n=53 spindle poles; unpaired two-tailed t-test, p=0.0018) **(Figure 1)**. Specifically, the average spindle pole area of control *RNAi* treated embryos was 14.6 μm^2 while that of *dyn-1 RNAi* treated embryos was 17.36 μm^2. Thus, our data have identified a novel role for the endocytic protein DYN-1 in regulating metaphase spindle pole assembly. To explore this role further, we examined the mechanism by which DYN-1 might regulate spindle assembly. One protein that is an important regulator of mitotic spindle pole assembly is the kinase PLK-1. Furthermore, PLK-1 exhibits a partially overlapping localization pattern with DYN-1 during mitosis (Chase *et al.,* 2000; Budirahardja and Gönczy, 2008; Martino *et al.,* 2017; Thompson *et al.,* 2002). Therefore, we questioned whether PLK-1 levels at the centrosomes were altered between control and *dyn-1 RNAi* treated embryos.

DYN-1 depletion increases the levels of centrosome-associated PLK-1

To determine whether DYN-1 depletion affects the levels of centrosome-associated PLK-1, we created a new *C. elegans* strain expressing mCherry-Tubulin and CRISPR-tagged endogenous PLK-1-sfGFP (Martino *et al.,* 2017) via genetic crossing. We then knocked down endogenous DYN-1 in this strain using *RNAi* and performed live imaging of control (*smd-1*) *RNAi* and *dyn-1 RNAi* treated embryos using spinning-disk confocal microscopy. Consistent with our hypothesis, our analysis revealed that PLK-1 levels at the centrosomes were elevated upon DYN-1 depletion **(Figure 2)**. Specifically, we found that the average PLK-1 fluorescence intensity in DYN-1-depleted embryos was 51.02 arbitrary units (n=40 centrosomes). This was about 1.5 times higher than that of control (*smd-1) RNAi* treated embryos (average PLK-1 fluorescence intensity = 33.13 arbitrary units; n=46 centrosomes; unpaired two-tailed t-test, $p<0.0001$). These data indicate that DYN-1 normally acts to negatively regulate PLK-1 localization to the centrosomes through an as-yet unidentified mechanism. Therefore, in the absence of DYN-1, PLK-1 is no longer restricted from localizing to the centrosomes and consequently, its levels at the centrosomes increase. These increased levels of centrosome-associated PLK-1 upon DYN-1 depletion **(Figure 2)** are consistent with the enlarged spindle poles that we observed upon DYN-1 depletion **(Figure 1).** However, it is currently unclear whether DYN-1 regulates PLK-1 localization via vesicular trafficking or through an endocytosis-independent mechanism. Future studies will be directed towards further dissecting the molecular mechanism by which DYN-1 regulates PLK-1 localization.

PLK-1 persists at the centrosomes following DYN-1 depletion in a subset of embryos during the later stages of mitosis

PLK-1 exhibits a spatially and temporally regulated localization during different stages of mitosis (Chase *et al.,* 2000; Budirahardja and Gönczy, 2008; Martino *et al.,* 2017). PLK-1

primarily localizes to the centrosomes and to the kinetochores from prophase to metaphase. Upon anaphase onset, PLK-1 starts re-localizing to the spindle midzone. Finally, during telophase, PLK-1 completely disappears from the centrosomes and is recruited to the midbody to facilitate abscission (Chase *et al.,* 2000; Budirahardja and Gönczy, 2008; Martino *et al.,* 2017). During the course of our imaging experiments, we noticed several embryos where PLK-1 appeared to persist at the centrosomes (specifically at the pericentriolar material) during telophase **(Figure 3A)**. To quantify this phenotype, we analyzed PLK-1 localization to the centrosomes at different cell cycle stages using maximum-intensity Z-projections of the time-lapse images from both control (*smd-1*) and *dyn-1 RNAi* treated embryos **(Figure 3B)**. Centrosomes where PLK-1 fluorescence intensity was visually determined to be above that of the background cytoplasmic PLK-1-sfGFP fluorescence were scored as being positive for PLK-1. Our analysis revealed that in control embryos at late telophase, there was no PLK-1 detectable at any of the centrosomes analyzed (n=48 centrosomes) **(Figure 3A and Figure 3B)**. In contrast, in 15% of the centrosomes from *dyn-1 RNAi* treated embryos (in 7 out of 48 centrosomes), PLK-1 was still detectable at the centrosomes at late telophase (Fisher's exact test, p=0.0124) **(Figure 3A and Figure 3B)**. We also noted a marked increase in the percentage of centrosomes with PLK-1 during early telophase upon DYN-1 depletion **(Figure 3B)**. Specifically, while only 13% of the centrosomes (6 out of 48 centrosomes) from control embryos had PLK-1 associated with them during early telophase, 40% of the centrosomes (19 out of 48 centrosomes) from DYN-1-depleted embryos still had PLK-1 associated with them at this stage (Fisher's exact test, p=0.0047) **(Figure 3B)**. These data suggest that a pool of PLK-1 tends to persist at the centrosomes of DYN-1-depleted embryos during the later stages of mitosis. Since DYN-1 depletion results in an elevation of PLK-1 levels at the centrosomes during early mitosis, it is

likely that these increased levels of PLK-1 make it difficult for PLK-1 to be effectively removed from the centrosomes during the later stages of mitosis in a subset of *dyn-1 RNAi* embryos.

DYN-1-depleted embryos exhibit abnormal midbody formation

Since DYN-1 has a known role in cytokinesis and localizes to the midbody (Thompson *et al.,* 2002), we analyzed midbody formation in DYN-1-depleted embryos using mCherry-tubulin fluorescence as a proxy for midbody assembly. We noted that all of the control *RNAi* treated embryos (n=26 embryos) exhibited a normal detectable bridge-like midbody during telophase as determined by intense tubulin fluorescence **(Figure 4A** (top panel, white arrow) **and Figure 4B)**. In contrast, 72% of the *dyn-1 RNAi* treated embryos (18 out of 25 embryos) either exhibited a defective midbody or did not exhibit any detectable midbody during telophase **(Figure 4A** (bottom panel) **and Figure 4B)** (Fisher's exact test, $p<0.0001$). In some of these instances, we observed that in DYN-1-depleted embryos, the midbody formed abnormally after telophase had already been completed and the embryo had entered the subsequent cell cycle. Together, these data suggest that DYN-1 function is required for proper midbody assembly.

PLK-1 localization to the midbody is defective in embryos depleted of DYN-1

Since our previous data demonstrated that PLK-1 continued to localize to the centrosomes at the later mitotic stages in a subset of DYN-1-depleted embryos **(Figure 3)**, we hypothesized that this may correlate with an abnormal localization of PLK-1 to the midbody during late mitosis. Indeed, time-lapse live imaging revealed that PLK-1-sfGFP localization to the midbody was defective in DYN-1 depleted embryos **(Figure 5)**. Specifically, we found that while all of the control embryos (n=26 embryos) exhibited a stereotypical localization of PLK-1-sfGFP at the center of the midbody, in about 72% of the DYN-1-depleted embryos (18 out of 25 embryos), PLK-1-sfGFP failed to localize correctly to the midbody **(Figure 5)** (Fisher's exact test,

p<0.0001). As reported previously, in some severe cases, the cleavage furrow failed to form completely upon DYN-1 depletion (Thompson *et al.,* 2002). In these cases, we observed that PLK-1-sfGFP localization was severely defective during both anaphase and telophase **(Supplementary Movie S1).** Notably, PLK-1-sfGFP failed to localize correctly to the midbody in 17 out of the 18 embryos that were quantified as having midbody defects in **Figure 4**. These data indicate that proper PLK-1 localization to the midbody is likely a prerequisite for normal midbody assembly.

Total protein levels of Plk1 are not increased upon DNM2 depletion in HeLa cells

Since we observed increased PLK-1 levels at the centrosomes upon DYN-1 depletion **(Figure 2)**, we asked whether this was occurring due to an overall increase in total PLK-1 levels or due to a specific enhancement of PLK-1-sfGFP localization to centrosomes. To answer this question, we performed western blot analysis of *C. elegans* whole worm lysates from control and *dyn-1 RNAi* worms and probed them for PLK-1-sfGFP. Unfortunately, we could not detect any PLK-1-sfGFP expression in our lysates, possibly due to its low abundance in whole worm lysates (data not shown). Since both PLK-1 and DYN-1 proteins are conserved between humans and *C. elegans* (Clustal Omega), we turned to HeLa cells to answer this question. We were able to successfully knockdown DNM2 (human DYN-1 homolog) in HeLa cells **(Figure S2A).** The DNM2 knockdown efficiency in our experiments ranged from ~81% to 95.4% **(Figure S2B)**. Normalized Plk1 expression levels measured from four independent experiments did not reveal a statistically significant increase in Plk1 levels upon DNM2 depletion **(Figure S2C)** (unpaired two-tailed t-test with Welch's correction, p=0.4516). These data support the notion that the total cellular levels of Plk1 are likely not increased upon DNM2 depletion.

In summary, our studies have identified a new role for the endocytic protein DYN-1 in regulating metaphase spindle assembly and PLK-1 localization during mitosis. Specifically, we find that upon DYN-1 depletion, PLK-1 accumulates at the centrosomes in metaphase and this is associated with aberrant metaphase spindle pole assembly. Furthermore, while PLK-1 is normally removed from the centrosomes during late mitosis, upon DYN-1 depletion, we find that PLK-1 persists at the centrosomes during the later stages of mitosis. We hypothesize that a failure to remove PLK-1 from the centrosomes in a timely manner likely causes midbody defects and results in cytokinesis failure in DYN-1-depleted embryos.

Moving forward, a detailed mechanistic analysis will be carried out to further investigate the cross-talk between DYN-1 and PLK-1. Specifically, we will utilize mutants such as *dyn-1(ky51ts)* to determine if the vesicular trafficking function of DYN-1 is required for this phenotype (Clark *et al.*, 1997; Grant and Hirsh 1999). Future experiments will be also designed to test if DYN-1 and PLK-1 physically interact or if perturbing the functions of other endocytic proteins phenocopies the DYN-1 depletion phenotype. We will also determine whether the localization of key cytokinesis regulators (e.g. CYK-4, NOP-1, NMY-2, ANI-1, RHO-1, ECT-2) is altered upon DYN-1 depletion. Rescue experiments involving partial knockdown of PLK-1 in *dyn-1 RNAi* embryos could potentially clarify whether elevated centrosomal PLK-1 levels contribute to the observed mitotic and cytokinetic defects of DYN-1 depletion. However, in our experience, achieving consistent and titratable knockdown of PLK-1 using *RNAi* by feeding has proven challenging. As a result, this experiment was not pursued in the present study. As an alternative, future studies will utilize the temperature-sensitive *plk-1(or683ts)* mutant to achieve partial loss of PLK-1 function under semi-permissive conditions (O'Rourke *et al.*, 2011). This allele was shown to remove PLK-1 from centrosomes in five hours at the restrictive temperature

223 of 25 °C (Martino *et al.,* 2017). To test whether reducing PLK-1 levels can rescue the cytokinesis
224 defects of *dyn-1*–depleted embryos, we will need to carefully titrate the inactivation window to
225 achieve centrosomal PLK-1 levels compatible with normal cell division. While promising, this
226 strategy is technically challenging, as it requires precise timing of embryo imaging within a
227 narrow window to achieve the optimal level of PLK-1 reduction. Despite these constraints, this
228 approach offers a powerful means to directly test whether elevated PLK-1 at centrosomes
229 underlies the mitotic and cytokinetic phenotypes observed upon DYN-1 depletion.

230 **MATERIALS AND METHODS**

231 ***C. elegans* strains growth and maintenance**

232 All *C. elegans* strains described in this study were grown and maintained using standard
233 techniques on OP50 seeded Modified Youngren's Only Bacto-peptone (MYOB) agar plates at
234 20ºC (the strains were shifted to other assay-specific temperatures as needed).

235 ***C. elegans* strains and genetic crosses**

236 The wild-type N2 strain and the OD2425 strain expressing PLK-1-sfGFP (*plk-1(lt18[plk-*
237 *1::sfGFP]::loxp) III)* (Martino *et al.,* 2017) were obtained from the *Caenorhabditis Genetics*
238 *Center* (CGC). The OC908 strain (*bsSi30[pCW9: unc-119(+) pcdk-11.2::sfgfp::his-58::cdk-11.2*
239 *3' UTR] II; bsIs20[pNP99: unc-119(+) tbb-1p::mCherry::tbb-2::tbb-2 3'-UTR]; bsIs2[pCK5.5:*
240 *Ppie-1::gfp::spd-2]*) and the OC779 strain (*bsSi15[pKO109: spd-2p-spd-2::mCherry::spd-2 3'-*
241 *utr, unc-119(+)] I; bsSi30[pCW9: unc-119(+) pcdk-11.2::sfgfp::his-58::cdk-11.2 3' utr] II; unc-*
242 *119(ed3) III*) were obtained from Dr. Kevin O'Connell's laboratory at NIDDK, NIH. The
243 mCherry–tubulin–expressing strain IYR028 (*bsIs20[pNP99: unc-119(+) tbb-1p::mCherry::tbb-*
244 *2::tbb-2 3'-UTR]*) was generated in our laboratory by crossing OC908 hermaphrodites with N2
245 males and isolating progeny carrying only the mCherry-tubulin transgene. Following this,

246 mCherry-tubulin expressing males were generated from the IYR028 strain by heat shock at 30°C
247 for 6 hours. These mCherry-tubulin males from the IYR028 strain were then crossed with PLK-
248 1-sfGFP expressing hermaphrodites from the OD2425 strain to generate the IYR038 strain
249 (*bsIs20[pNP99: unc-119(+) tbb-1p::mCherry::tbb-2::tbb-2 3'-UTR]; plk-1(lt18[plk-*
250 *1::sGFP]::loxP) III)* which was homozygous for both mCherry-Tubulin and PLK-1-sfGFP. This
251 IYR038 strain was used for all but one of the imaging experiments described in this study. The
252 experiment involving the analysis of cytokinesis failure utilized the OC779 strain expressing
253 mCherry SPD-2 and GFP-histone.

254 ***RNAi* by feeding**

255 HT115 bacteria expressing the *dyn-1 RNAi* construct were purchased from Horizon Discovery
256 Ltd. (Lafayette, CO) while HT115 bacteria expressing the *smd-1 RNAi* construct (control) were
257 obtained from Dr. Kevin O'Connell's laboratory (NIDDK, Bethesda, MD). HT115 *E. coli*
258 transformed with either control (*smd-1)* or *dyn-1 RNAi* plasmids were grown on MYOB plates
259 supplemented with 50 µg/ml carbenicillin and 2 mM Isopropyl β- d-1-thiogalactopyranoside
260 (IPTG) as described previously (Kamath and Ahringer J 2003; Iyer *et al.,* 2022). Briefly, L4-
261 stage *C. elegans* from either the IYR038 or the OC779 strains were transferred onto the
262 respective *RNAi* plates and incubated at 25 ºC for 24 to 36 hours. Gravid adults from these plates
263 were then dissected to release their embryos and 1-cell stage embryos were analyzed by confocal
264 live imaging.

265 ***C. elegans* embryo live imaging using a spinning-disk confocal microscope**

266 *C. elegans* embryos obtained from dissected *smd-1* and *dyn-1 RNAi* treated worms were imaged
267 using an Olympus Yokagawa X1 spinning-disk confocal microscope as described previously
268 (Bergwell *et al.,* 2023) with a few alterations. Timelapse imaging was performed using the

269 cellSens software (Olympus America Inc.) by taking 1.5 µm Z-stacks every ~75 seconds at a
270 60X magnification with a 1.42 numerical aperture (NA) objective using a Prime 95B CMOS
271 camera. To enable quantitative analysis, all images were captured at the same laser intensity
272 (50% laser intensity for both 561 nm and 488 nm channels) and exposure time (700 msec
273 exposure time for both 561 nm and 488 nm channels). Maximum intensity Z-projections were
274 obtained using the cellSens software and converted to a .png format for all representative images
275 and analyses. All brightness and contrast adjustments were applied equally for both the control
276 and *dyn-1 RNAi* representative images to enable better image presentation and viewing.

277 **Cytokinesis failure quantification**

278 To score cytokinesis failure, the development of each embryo was monitored from the 1-cell
279 stage to the 4-cell stage. If the embryonic nuclei coalesced back to set up a multipolar spindle at
280 the 2-cell stage, the embryo was scored as having failed cytokinesis.

281 **Spindle pole area measurement**

282 To measure spindle pole area, the cellSens software (Olympus America Inc.) was used to obtain
283 maximum intensity Z-projections of the original .vsi files. These Z-projections were saved in a
284 .png format with the fixed scaling (left:80 and right:400) for all images and further analyzed
285 using the Nikon NIS-Elements software (Nikon Instruments Inc.). The calibration on the NIS-
286 Elements software was set to 1 pixel = 0.183 µm. The thresholding tool in NIS-Elements was
287 used to define and compute the spindle pole area (in μm^2) (intense mCherry-tubulin fluorescence
288 demarcated each spindle pole). Only regions with clearly defined spindle poles were included in
289 the analysis. Embryos in which spindle poles could not be reliably distinguished were excluded.

290 **PLK-1 metaphase centrosome intensity measurements**

291 In our time-lapse imaging experiments, the stage immediately prior to anaphase onset (~75
292 seconds before anaphase) was designated as metaphase. Notably, there was some embryo-to-
293 embryo variability in chromosome alignment at this stage; in some embryos, the chromosomes
294 were centrally aligned, while in others, they were still in the process of aligning. To quantify
295 PLK-1–sfGFP fluorescence at the centrosomes, .avi files of maximum intensity Z-projections of
296 metaphase embryos were analyzed using Nikon NIS-Elements software (Nikon Instruments,
297 Inc.), with image calibration set to 1 pixel = 0.183333 µm. A region of interest (ROI) measuring
298 13.81 μm^2 was drawn around each centrosome and within the cytoplasm of the same embryo.
299 Cytoplasmic PLK-1–sfGFP intensity was then subtracted from centrosomal PLK-1-sfGFP
300 intensity to calculate the mean PLK-1-sfGFP fluorescence intensity, reported in arbitrary units.
301 Embryos with inaccurate PLK-1-sfGFP fluorescence due to debris on top of the embryo
302 affecting maximum intensity Z-projections were excluded from our analysis. Embryos where the
303 centrosomal PLK-1–sfGFP signal could not be clearly distinguished from the chromosomal
304 PLK-1-sfGFP signal were also excluded from our analysis.

305 **Analysis of PLK-1 persistence at centrosomes**

306 To analyze PLK-1-sfGFP persistence at centrosomes, maximum intensity Z-projections of each
307 timelapse sequence were visually analyzed for the presence or the absence of PLK-1-sfGFP at
308 the centrosomes. Centrosomes where the fluorescence intensity of PLK-1-sfGFP was visually
309 determined to be greater than the cytoplasmic background PLK-1-sfGFP fluorescence were
310 scored as being positive for PLK-1-sfGFP. The cell cycle stages were classified as follows:
311 metaphase: the chromosomes were aligning at the center of the cell and a diamond-shaped
312 spindle was formed, early anaphase: ~75 seconds after metaphase when the chromosomes start to

313 separate, late anaphase: ~75 seconds after early anaphase, early telophase: ~75 seconds after late
314 anaphase and late telophase: ~75 seconds after early telophase.

315 **Quantification of midbody abnormalities**

316 Maximum intensity Z-projections of the 561 (red) channel from the imaged IYR038 strain were
317 analyzed for midbody defects. Midbody assembly was analyzed at either 300 or 375 seconds
318 after metaphase onset. A normal midbody was classified as a structure where an intense tubulin
319 bridge was clearly visible at the abscission area close to the center of the embryo. An abnormal
320 midbody was defined as one where either no intense tubulin bridge connecting the two daughter
321 cells was detected or where a structure resembling the midbody formed after the cell had already
322 entered the next cell cycle.

323 **Quantification of PLK-1 midbody localization defects**

324 Maximum intensity Z-projections were used to quantify PLK-1-sfGFP midbody localization
325 defects. PLK-1-sfGFP localization to the midbody was analyzed at either 300 or 375 seconds
326 after metaphase onset. Embryos where a bright PLK-1-sfGFP spot could be detected at the
327 abscission point during early to late telophase were classified as exhibiting a normal PLK-1
328 midbody localization. Embryos where PLK-1-sfGFP exhibited a scattered localization at the
329 cleavage furrow during early to late telophase were classified as exhibiting an abnormal PLK-1
330 localization.

331 **Statistical analysis of *C. elegans* studies**

332 Graphpad prism 10.5 (GraphPad Software, Inc., San Diego, CA) was used to perform statistical
333 analyses of all the data. For all the data, error bars represent the standard deviation (s.d.) above
334 and below the mean and the middle lines represent the mean. p-values were rounded to two
335 decimal places and considered significant if $p<0.05$. A two-tailed unpaired t-test was used to

336 analyze the spindle pole area and the PLK-1-sfGFP fluorescence intensity data. A two-tailed
337 unpaired t-test with Welch's correction was used to analyze band intensities from western
338 blotting. A Fisher's exact test was used to analyze the cytokinesis defects, PLK-1-sfGFP
339 persistence at the centrosomes, defects in midbody formation and defects in PLK-1-sfGFP
340 localization to the midbody.

341 **Cell culture and siRNA transfections**

342 HeLa cells were maintained by culturing them in Dulbecco's Modified Eagle Medium (DMEM)
343 (Gibco, Catalog #11-995-040) with 10% fetal bovine serum (FBS) (Corning, Catalog
344 #MT35010CV) and 1% penicillin/streptomycin (1% P/S) (Gibco, Catalog #15-140-122) in a
345 37°C incubator with 5% CO_2. For DNM2 siRNA experiments, HeLa cells were seeded at a
346 density of up to $2.4X10^5$ cells per well (20 to 30% confluence) into each well of a 6-well plate
347 and allowed to adhere to the plate for 24 hours prior to transfection. The cells were rinsed twice
348 with DPBS (Gibco, Catalog # 14040-117) prior to transfection. Control and DNM2 siRNA
349 constructs were obtained from Santa Cruz Biotechnology Inc. (Control siRNA Catalog # sc-
350 37007; DNM2 siRNA Catalog # sc-35236). The siRNA constructs were transfected into HeLa
351 cells using Lipofectamine LTX reagent (Thermo Fisher Scientific, Inc., Catalog # 15-338-030) in
352 1 ml of reduced serum OPTI-MEM medium (Gibco, Catalog # 31985070) according to the
353 manufacturer's instructions. After six hours, 1 ml of DMEM containing 20% FBS and 2% P/S
354 was added to the transfected cells. After 24 hours, the media containing the transfection reagent
355 was removed and replaced with fresh DMEM with 10%FBS and 1% P/S. The cells were allowed
356 to grow for 48 hours and then lysed with RIPA buffer (Santa Cruz Biotechnology Inc, Catalog #
357 sc-24948A) containing 1 mM phenylmethylsulfonyl fluoride (PMSF) (Thermo Fisher Scientific,
358 Inc., Catalog # 36978) and a protease inhibitor cocktail (Pierce Protease Inhibitor Tablets,

359 EDTA-free, Catalog #A32965). Lysate protein concentrations were measured using a Bradford
360 assay (Thermo Scientific Inc., Catalog # 23200).

361 **Western blotting**

362 The HeLa cell lysates from control and DNM2 siRNA treated cells were subjected to western
363 blot analysis using the Bio-Rad wet transfer method. Briefly, approximately 20 micrograms of
364 protein from each sample were loaded onto a well of an SDS-PAGE gel (Genscript Corporation,
365 Catalog # M00656). The gel was run until adequate protein separation was achieved. Following
366 electrophoresis, the proteins were subjected to an overnight transfer onto a 0.2 µm nitrocellulose
367 membrane (Thermo Fisher Scientific Inc., Catalog # LC2000) for 16 hours at 30V using the
368 Towbin buffer (25 mM Tris base, 192 mM Glycine, 20% (v/v) Methanol) at 4ºC. The membrane
369 was then stained with the Ponceau S solution (Fisher Scientific Inc. Catalog # A40000279) to
370 ensure good protein transfer. Following this, the membranes were blocked with blocking buffer
371 (1X Tris-buffered saline (TBS) (0.05 M Tris, 0.15 M sodium chloride, pH=7.4), 0.2% gelatin
372 from cold water fish skin (Sigma-Aldrich Inc., Catalog # G7041), 0.1% Tween 20 (Thermo
373 Scientific Inc., Catalog # J20605-AP) and 0.02% sodium azide (RPI Research Products, Catalog
374 # S24080-250)) at room temperature for 30 minutes. Once blocked, the membranes were probed
375 with a rabbit polyclonal anti-DNM2 antibody at a 1:1000 dilution (Abcam Inc., Catalog #
376 ab3457), a mouse monoclonal anti-tubulin antibody at a 1:100 dilution (Santa Cruz
377 Biotechnology Inc., Catalog # sc-32293), a mouse monoclonal anti-Plk1 antibody at a 1:100
378 dilution (Santa Cruz Biotechnology Inc., Catalog # sc-17783) for 2 hours at room temperature.
379 Subsequently, the membrane was washed 3 times with 1X TBS supplemented with 0.1% Tween-
380 20 (1XTBST) and incubated with the corresponding secondary antibodies (IRDye 680RD goat
381 anti-rabbit IgG secondary antibody (LI-COR Biotech, LLC, Catalog # 926-68071) and IRDye

382 800CW donkey anti-mouse IgG secondary antibody (LI-COR Biotech, LLC, Catalog # 926-
383 32212)) at a 1:10,000 dilution for 1 hour at room temperature. The membrane was washed again
384 3 times using 1XTBST and imaged using the LI-COR Odyssey Fc imaging system (LI-COR
385 Biotech, LLC).

386 **Western blot intensity analysis**

387 The band intensities for the different proteins were quantified using the LI-COR Image Studio
388 software (LI-COR Biotech LLC) and normalized with respect to the loading control (tubulin).
389 Band intensities from four independent western blot experiments were analyzed and plotted.

390 **ACKNOWLEDGMENTS**

391 This work was supported by NIH/NIGMS grant 5P20GM103636-09 and start-up funding from
392 North Carolina A&T State University to J.I. Additional support was provided by NIH/NIGMS
393 grant 1R35GM153737 and NCI grant 1R01CA273095 (to R.N.). We thank the University of
394 Tulsa for supporting Livinus Anyanwu and for providing infrastructure used in several
395 experiments. OC908 and OC779 strains were generously provided by Dr. Kevin O'Connell
396 (NIDDK, NIH). Some of the strains used in this study were provided by the CGC, which is
397 funded by NIH Office of Research Infrastructure Programs (P40 OD010440). The authors
398 declare no competing interests.

399 **REFERENCES**

400 Archambault V, Glover DM (2009). Polo-like kinases: conservation and divergence in their
401 functions and regulation. **Nat Rev Mol Cell Biol** *10*(4), 265-275.

402 Arnaud L, Pines J, Nigg EA (1998). GFP tagging reveals human Polo-like kinase 1 at the
403 kinetochore/centromere region of mitotic chromosomes. **Chromosoma** *107*(6), 424-429.

404 Bergwell M, Smith A, Smith E, Dierlam C, Duran R, Haastrup E, Napier-Jameson R, Seidel R,
405 Potter W, Norris A, *et al.* (2023). A primary microcephaly-associated sas-6 mutation perturbs
406 centrosome duplication, dendrite morphogenesis, and ciliogenesis in Caenorhabditis
407 elegans. **Genetics** *224*(4), p.iyad105.
408 Brennan IM, Peters U, Kapoor TM, Straight AF (2007). Polo-like kinase controls vertebrate
409 spindle elongation and cytokinesis. **PloS one** *2*(5), e409.
410 Budirahardja Y, Gönczy P (2008). PLK-1 asymmetry contributes to asynchronous cell division
411 of *C. elegans* embryos. **Development** *135*(7), 1303–1313.
412 Burkard ME, Randall CL, Larochelle S, Zhang C, Shokat KM, Fisher RP, Jallepalli PV (2007).
413 Chemical genetics reveals the requirement for Polo-like kinase 1 activity in positioning RhoA
414 and triggering cytokinesis in human cells. **Proc Natl Acad Sci USA** *104*(11), 4383-4388.
415 Burkard ME, Maciejowski J, Rodriguez-Bravo V, Repka M, Lowery DM, Clauser KR, Zhang C,
416 Shokat KM, Carr SA, Yaffe MB, *et al.* (2009). Plk1 self-organization and priming
417 phosphorylation of HsCYK-4 at the spindle midzone regulate the onset of division in human
418 cells. **PLoS Biol** *7*(5), p.e1000111.
419 Chase D, Serafinas C, Ashcroft N, Kosinski M, Longo D, Ferris DK, Golden, A (2000). The
420 polo-like kinase PLK-1 is required for nuclear envelope breakdown and the completion of
421 meiosis in Caenorhabditis elegans. **Genesis**, *26*(1), 26-41.
422 Clark SG, Shurland DL, Meyerowitz EM, Bargmann CI, Van Der Bliek AM (1997). A dynamin
423 GTPase mutation causes a rapid and reversible temperature-inducible locomotion defect in C.
424 elegans. **Proc Natl Acad Sci USA** *94*(19), 10438-10443.

425 Golsteyn RM, Mundt KE, Fry AM, Nigg EA (1995). Cell cycle regulation of the activity and
426 subcellular localization of Plk1, a human protein kinase implicated in mitotic spindle function. **J**
427 **Cell Biol** *129*(6), 1617-1628.
428 Grant B, Hirsh D (1999). Receptor-mediated endocytosis in the Caenorhabditis elegans
429 oocyte. **Mol Biol Cell** *10*(12), 4311-4326.
430 Hinshaw JE (2000). Dynamin and its role in membrane fission. **Annu Rev Cell Dev** *16*(1), 483-
431 519.
432 Iyer J, Gentry LK, Bergwell M, Smith A, Guagliardo S, Kropp PA, Sankaralingam P, Liu Y,
433 Spooner E, Bowerman B, *et al.* (2022). The chromatin remodeling protein CHD-1 and the EFL-
434 1/DPL-1 transcription factor cooperatively down regulate CDK-2 to control SAS-6 levels and
435 centriole number. **PLoS Genet** *18*(4), p.e1009799.
436 Kamath RS, Ahringer J (2003). Genome-wide RNAi screening in Caenorhabditis elegans.
437 **Methods** *30*(4), 313-321.
438 Khurana H, Pucadyil TJ (2023). “Gearing” up for dynamin-catalyzed membrane fission. **Curr**
439 **Opin Cell Biol** *83*, 102204.
440 Kishi K, Van Vugt MA, Okamoto KI, Hayashi Y, Yaffe MB (2009). Functional dynamics of
441 Polo-like kinase 1 at the centrosome. **Mol Cell Biol** *29*(11), 3134-3150.
442 Lee KS, Yuan YLO, Kuriyama R, Erikson RL (1995). Plk is an M-phase-specific protein kinase
443 and interacts with a kinesin-like protein, CHO1/MKLP-1. **Mol Cell Biol** *15*(12), 7143-7151.
444 Martino L, Morchoisne-Bolhy S, Cheerambathur DK, Van Hove L, Dumont J, Joly N, Desai A,
445 Doye V, Pintard L (2017). Channel nucleoporins recruit PLK-1 to nuclear pore complexes to
446 direct nuclear envelope breakdown in C. elegans. **Dev Cell** *43*(2), 157-171.

447 Menon M, Schafer DA (2013). Dynamin: expanding its scope to the cytoskeleton. **Int Rev Cell**
448 **Mol Biol** *302*, 187-219.
449 Nishi Y, Rogers E, Robertson SM, Lin R (2008). Polo kinases regulate C. elegans embryonic
450 polarity via binding to DYRK2-primed MEX-5 and MEX-6. **Development** *135*(4), 687–697.
451 O'Rourke SM, Carter C, Carter L, Christensen SN, Jones MP, Nash B, Price MH, Turnbull DW,
452 Garner AR, Hamill DR, *et al.* (2011). A survey of new temperature-sensitive, embryonic-lethal
453 mutations in C. elegans: 24 alleles of thirteen genes. **PLoS One** 6, e16644.
454 Pelissier A, Chauvin JP, Lecuit T (2003). Trafficking through Rab11 endosomes is required for
455 cellularization during Drosophila embryogenesis. **Curr Biol** *13*(21), 1848-1857.
456 Petronczki M, Glotzer M, Kraut N, Peters JM (2007). Polo-like kinase 1 triggers the initiation of
457 cytokinesis in human cells by promoting recruitment of the RhoGEF Ect2 to the central
458 spindle. **Dev Cell** *12*(5), 713-725.
459 Petronczki M, Lénárt P, Peters JM (2008). Polo on the rise—from mitotic entry to cytokinesis
460 with Plk1. **Dev Cell** *14*(5), 646-659.
461 Santamaria A, Neef R, Eberspächer U, Eis K, Husemann M, Mumberg D, Prechtl S, Schulze V,
462 Siemeister G, Wortmann L, *et al*. (2007). Use of the novel Plk1 inhibitor ZK-thiazolidinone to
463 elucidate functions of Plk1 in early and late stages of mitosis. **Mol Biol Cell** *18*(10), 4024-4036.
464 Schmucker S, Sumara I (2014). Molecular dynamics of PLK1 during mitosis. **Mol Cell Oncol**
465 *1*(2), e954507.
466 Shpetner HS, Vallee RB (1989). Identification of dynamin, a novel mechanochemical enzyme
467 that mediates interactions between microtubules. **Cell** *59*(3), 421-432.

468 Thompson HM, Skop AR, Euteneuer U, Meyer BJ, McNiven MA (2002). The large GTPase
469 dynamin associates with the spindle midzone and is required for cytokinesis. **Curr Biol**, *12*(24),
470 2111-2117.
471 Wienke DC, Knetsch ML, Neuhaus EM, Reedy MC, Manstein DJ (1999). Disruption of a
472 dynamin homologue affects endocytosis, organelle morphology, and cytokinesis in
473 Dictyostelium discoideum. **Mol Biol Cell** *10*(1), 225-243.
474 Wolfe BA, Takaki T, Petronczki M, Glotzer M (2009). Polo-like kinase 1 directs assembly of the
475 HsCyk-4 RhoGAP/Ect2 RhoGEF complex to initiate cleavage furrow formation. **PLoS**
476 **Biol** *7*(5), e1000110.
477 Zitouni S, Nabais C, Jana SC, Guerrero A, Bettencourt-Dias M (2014). Polo-like kinases:
478 structural variations lead to multiple functions. **Nat Rev Mol Cell Biol** *15*(7), 433-452.

Figure 1

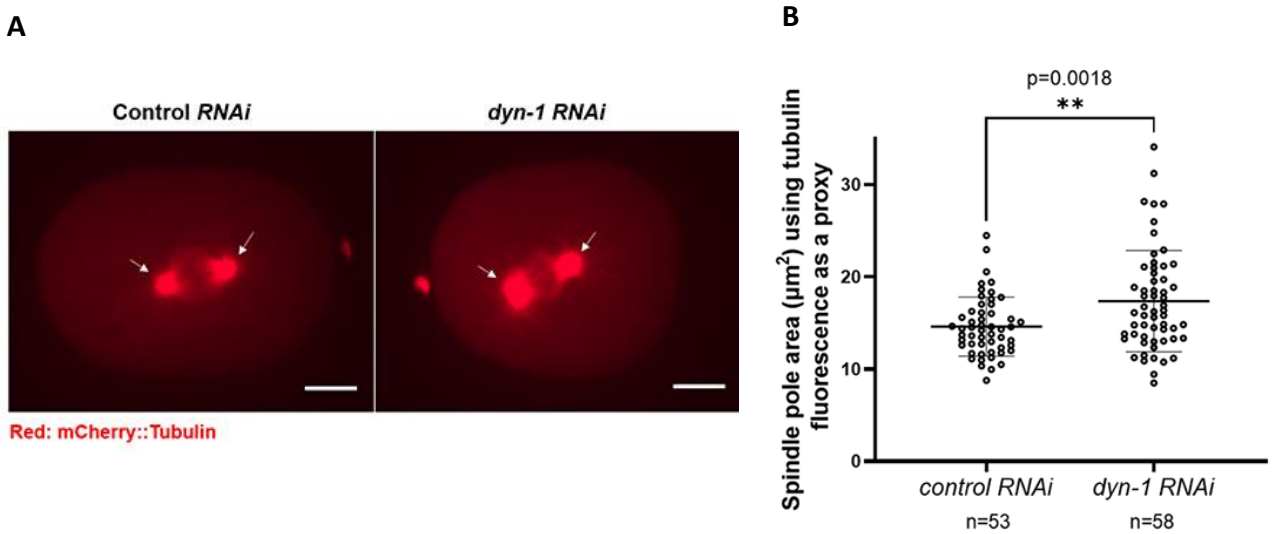

Figure 1: DYN-1 depletion increases spindle pole size. (A) Stills from live imaging of *C. elegans* embryos demonstrating that spindle pole size is increased upon *dyn-1 RNAi*. White arrows highlight spindle poles. Scale bar = 10 µm. (B) Quantification of spindle pole area in control and DYN-1-depleted embryos using mCherry-tubulin fluorescence as a proxy for the spindle poles. Each circle represents the area of a single spindle pole. n = number of spindle poles analyzed. Error bars represent the s.d; middle lines represent the mean. Unpaired two-tailed t-test, p=0.0018.

Figure 2

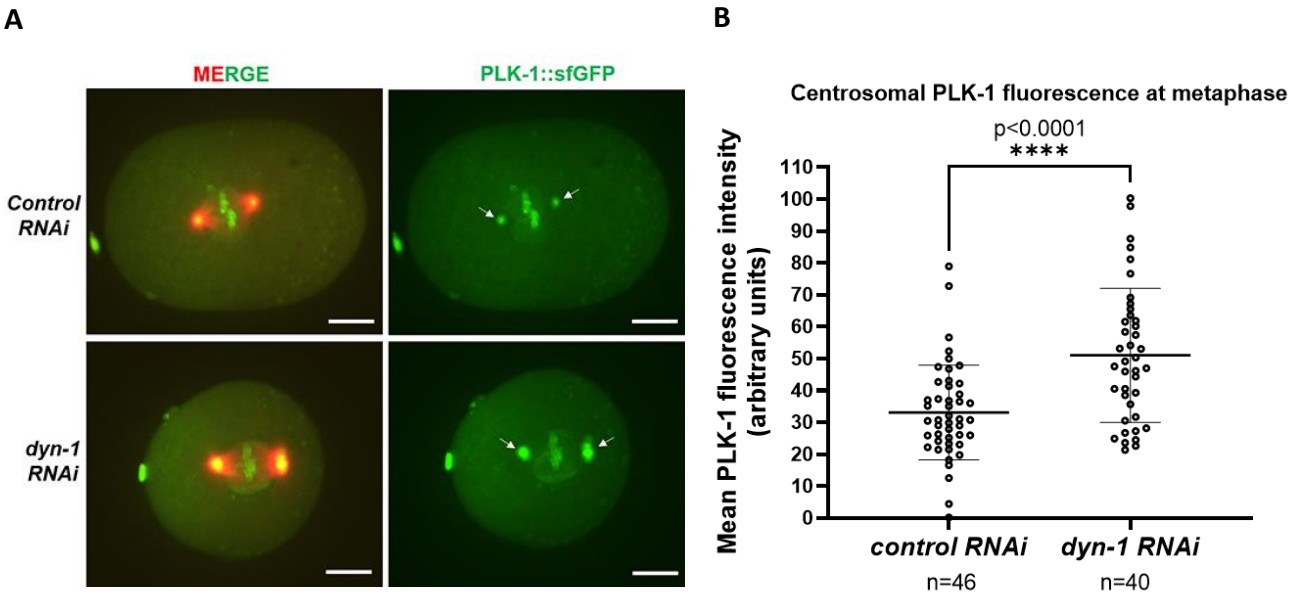

Figure 2: DYN-1 depletion increases centrosomal PLK-1-sfGFP localization. (A) Stills from live imaging assays of *C. elegans* embryos expressing PLK-1-sfGFP (green) and mCherry-tubulin (red) demonstrating that centrosomal localization of PLK-1-sfGFP is increased upon *dyn-1* depletion. White arrows represent centrosome-localized PLK-1. Scale bar = 10 µm. (B) Quantification of PLK-1-sfGFP fluorescence intensity upon control and *dyn-1 RNAi*. Each circle represents the PLK-1-sfGFP fluorescence intensity at a single centrosome. n = number of centrosomes analyzed. Error bars represent the s.d; middle lines represent the mean. Unpaired two-tailed t-test, $p<0.0001$.

Figure 3

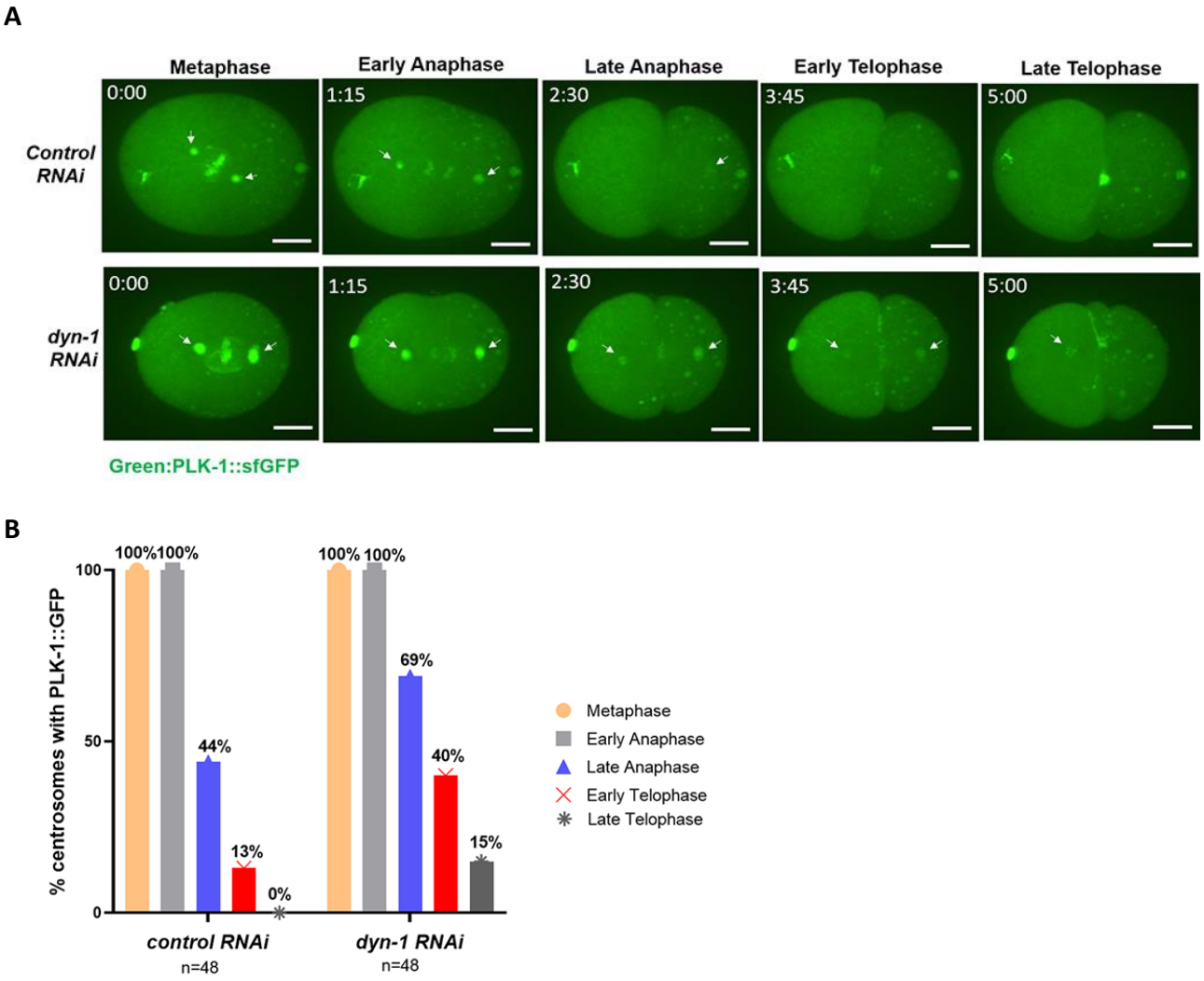

Figure 3: PLK-1-sfGFP persists at the centrosomes upon *dyn-1* knockdown (A) Stills from live imaging experiments of *C. elegans* embryos expressing PLK-1-sfGFP (green) demonstrating that PLK-1-sfGFP persists at the centrosomes upon *dyn-1* depletion. The metaphase timepoint was annotated as the zero timepoint. White arrows represent PLK-1-sfGFP at centrosomes. Scale bar = 10 µm. (B) Quantification of PLK-1-sfGFP localization at the centrosomes at different cell cycle stages. n = number of centrosomes analyzed.

Figure 4

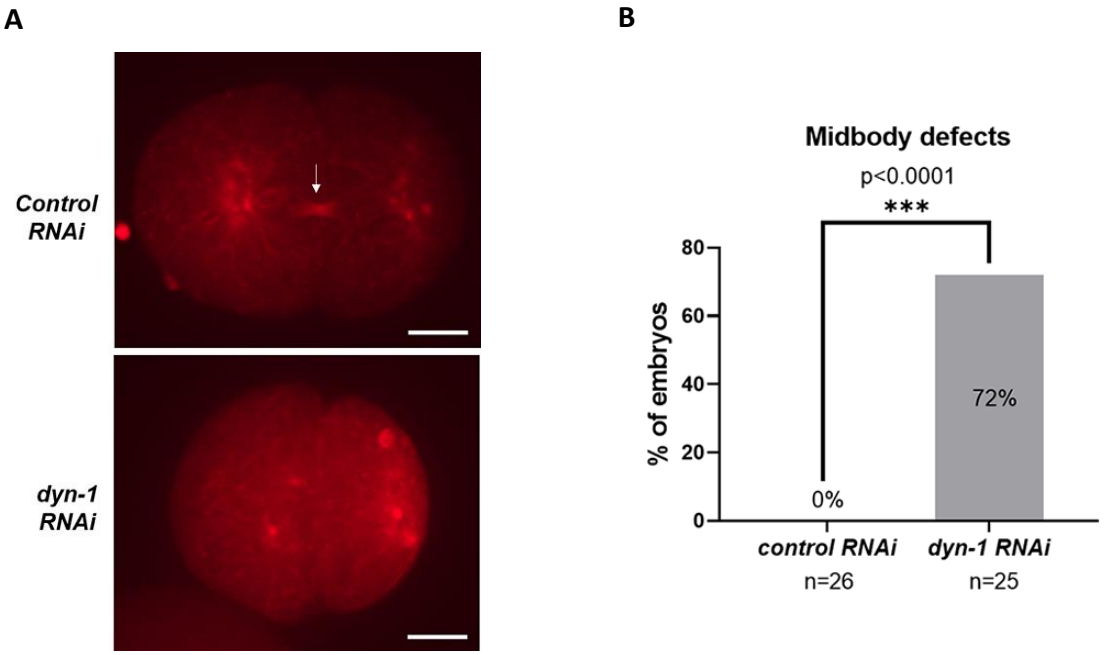

Figure 4: DYN-1 knockdown causes midbody defects. (A) Stills from live imaging of *C. elegans* embryos demonstrating that midbody assembly is defective upon DYN-1 depletion. Red: mCherry-tubulin, the white arrow represents a normal midbody. Scale bar = 10 µm. (B) Quantification of midbody defects observed upon *dyn-1* depletion. n= number of embryos analyzed. Fisher's exact test, $p<0.0001$.

Figure 5

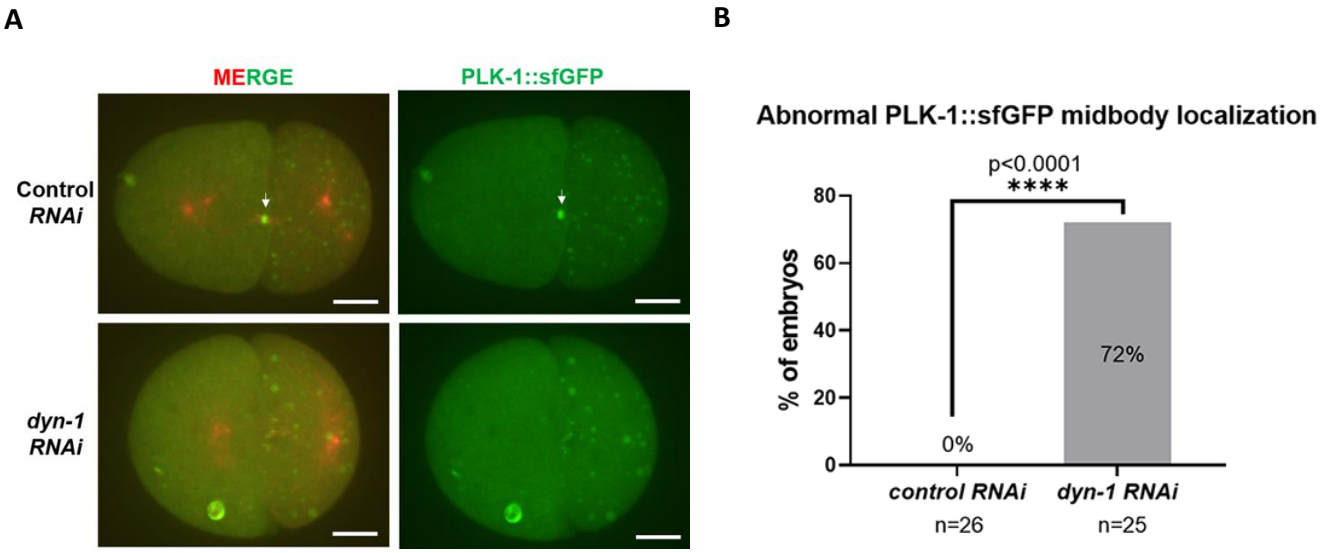

Figure 5: PLK-1-sfGFP fails to localize correctly to the midbody upon *dyn-1 RNAi*. (A) Stills from live imaging of *C. elegans* embryos expressing PLK-1-sfGFP (green) and mCherry-tubulin (red) demonstrating that the midbody localization of PLK-1 is perturbed upon *dyn-1* depletion. The white arrow represents a normal PLK-1 localization at the midbody. Scale bar = 10 µm. (B) Quantification of PLK-1-sfGFP midbody localization upon *dyn-1 RNAi*. n = number of embryos analyzed. Fisher's exact test, $p<0.0001$.